J Solid State Electrochem (2016) 20:1527–1538
DOI 10.1007/s10008-016-3166-y

ORIGINAL PAPER

Dip-coating deposition of resistive $BiVO_4$ thin film and evaluation of their photoelectrochemical parameters under distinct sources illumination

M. R. da Silva [1,2] · L. V. A. Scalvi [2] · V. S. L. Neto [3] · L. H. Dall'Antonia [3]

Received: 28 October 2015 / Revised: 14 February 2016 / Accepted: 19 February 2016 / Published online: 27 February 2016

Abstract Resistive monoclinic bismuth vanadate ($BiVO_4$) nanocrystals in the form of thin films were obtained by the solution combustion synthesis coupled with the dip-coating deposition process. The structure, morphology, and optical properties of $BiVO_4$ nanocrystals were characterized by means of x-ray diffraction (XRD), scanning electron microscopy (SEM), and UV-Vis spectroscopy. The photoelectrochemical properties were obtained by cyclic voltammetry and chronoamperometry techniques in potassium chloride (KCl) electrolyte solution under distinct visible light sources irradiation condition. Under blue InGaN light emitting diode (LED) irradiation, the electrode has a better efficiency, faster response time (260 ms), and faster decay time (65 ms), when compared with the irradiation by dichroic lamp. Besides, the photocurrent density (j_{ph}) is approximately 39 times higher than j_{ph} obtained under dichroic lamp. The performance analysis based on the methylene blue degradation reaction has shown that the $BiVO_4$ material has higher electroactivity under InGaN LED irradiation condition, with estimated k_{obs} value of 200×10^{-4} min^{-1}, which is a little higher than the value obtained with dichroic lamp illumination. In the dark condition, the $BiVO_4$ presented much lower photocatalytic activity.

✉ M. R. da Silva
marcelors@feb.unesp.br

[1] Engineering College, UNESP – São Paulo State University, CTI, Bauru, São Paulo, Brazil

[2] Department of Physics – FC, UNESP – São Paulo State University, Bauru, São Paulo, Brazil

[3] Department of Chemistry, UEL – State University of Londrina, Londrina, Paraná, Brazil

Keywords Resistive · $BiVO_4$ · Thin film · InGaN LED · Dichroic lamp

Introduction

In recent years, bismuth vanadate ($BiVO_4$), an n-type semiconductor material in the monoclinic phase, has drawn great attention because of their ability for photocatalysis under sunlight absorption [1–7]. In the monoclinic $BiVO_4$ structure, the band gap energy is rather narrow, approximately 2.4 eV, due to the presence of empty 3d orbital of vanadium coupled to 2p orbital of oxygen and 6p of bismuth, resulting in a conduction band minimum at the Brillouin zone edge, favorable to low-energy direct transition [4, 7–9].

Previously published papers have dealt with the photocatalytic properties of monoclinic $BiVO_4$ phase face to the degradation of organic pollutants in aqueous media, when under visible light irradiation [7, 10–14]. Besides partial photocatalytic water splitting reaction has also been accomplished, driving the oxygen evolution by photogenerated holes on valence band [8, 15–19]. Recently, nanostructured $BiVO_4$ thin film has been used as photoanode electrode in a photoelectrochemical system [7, 10, 20–22]. In the photoelectrochemical configuration system, the electrochemical potential applied to the working electrode forces the electron flow, which in this case is photogenerated by means of visible light irradiation, towards the counter-electrode, preventing the fast electron–hole recombination–back process [7, 10]. The effect of photogenerated charge carriers separation with high efficiency is the key to the high quantum efficiency of the photoanode, leading to an improved photoelectrochemical performance of system.

Numerous techniques have been employed for obtaining $BiVO_4$ semiconductor material [7, 8, 13, 16, 18, 21, 23]. Among all the available processes, the solution combustion

synthesis (SCS) technique may be selected due to its simplicity and versatility for obtaining $BiVO_4$ nanocrystals with monoclinic structure and relatively low cost process [23–29]. However, as many other semiconductor oxides, the $BiVO_4$ obtained by this process presents a rather high electrical resistivity [30–32].

Considering the electrochemical system, the photo-induced current density is influenced by electrolyte solution and by excitation energy. Appropriate excitation energy, which in this case must be about the band gap energy, may lead to stable photo-induced current density. The electrolyte solution is a fundamental parameter to investigate the decay profile and response time of photo-induced current density [7, 10]. Some previously published papers [7, 10, 16] show that the $BiVO_4$ thin film electrode is more electroactive in sodium sulfate electrolyte solution because ions SO_4^{-2} are more easily oxidized than other electrolyte solutions and water molecules.

In this context, this paper deals with the investigation of photoelectrochemical properties of resistive monoclinic $BiVO_4$ nanocrystalline thin films deposited on conducting fluorine-doped tin oxide (FTO) substrate through the SCS technique along with the dip-coating deposition process. The photoelectrochemical properties were investigated by excitation with different visible light sources: a dichroic lamp and a blue InGaN light emitting diode (LED). Besides, this paper brings a deep investigation of the decay of photo-induced current density, carried out through chronoamperometry measurements. To our knowledge, the influence of different visible light sources on photoelectrochemical properties of $BiVO_4$ electrode has not been used by other research groups. This is particularly accurate for the decay of photo-induced current using KCl electrolyte solution, which is analyzed here.

Experimental

Synthesis of resistive monoclinic phase $BiVO_4$ thin film

The monoclinic phase of $BiVO_4$ was obtained by the solution combustion synthesis (SCS) technique, adapted from widely published procedures [23–29]. A scheme showing the experimental procedure of the $BiVO_4$ thin films synthesis can be seen in Fig. 1a. First, a bismuth precursor solution was prepared by adding 2.5 g of $Bi(NO_3)_3{\cdot}6H_2O$ (Sigma-Aldrich, p.a.) and 1.0 g of citric acid (Sigma-Aldrich, p.a.), which were dissolved in 70 mL of 1.5 mol L^{-1} HNO_3 (Sigma-Aldrich, p.a.), leading to a colorless solution. Then, the pH of this solution was adjusted to 7–8 by dripping concentrated ammonium hydroxide (NH_4OH, Sigma-Aldrich, p.a.). Finally, 1.5 g of urea is added, which plays the role of combustible for the self-sustainable reaction of the SCS technique [25–27]. On the other hand, as part of the synthesis process, the vanadium precursor solution was prepared by adding 1.0 g of citric acid and 0.5 g of $(NH_4)_3VO_4$ (Sigma-Aldrich, p.a.), which was dissolved in 70 mL of deionized water at 80 °C, remaining under stirring for 20 min, giving origin to a yellowish solution. The colorless and yellowish solutions were mixed together and left in a muffle furnace at 85 °C for 20 h, giving birth to a material with gel consistency and intense blue-green color. This blue-green gel was diluted in 50 mL of deionized water, resulting in a bluish green solution that was called working solution. The dip-coating process was used to deposit $BiVO_4$ thin film on a fluorine-doped tin oxide (FTO) conductor substrate, where the substrate is sequentially dipped according to the desired number of layers, by using the dip rate of 10 cm min^{-1}. Between each deposited layer, the sample is dried for 10 min in room atmosphere, followed by heating at 400 °C for another 10 min. When the desired number of layers is reached (in the present case, it used ten layers), the film is thermally annealed at 400 °C for 4 h. Finally, a $BiVO_4$ thin film with yellowish color is obtained. In order to get $BiVO_4$ material in the powder form, the blue-green gel was thermally treated at 600 °C for 4 h.

Physical characterization

X-ray diffraction (XRD) measurements were carried out using a PANalytical diffractometer, model X'Pert PRO MPD, with the CuKα (1.5418 Å) radiation, coupled to a nickel filter, in order to reduce the unfavorable CuKβ radiation. The applied tension was 40 kV and the current was 30 mA. The scanning range was from 10 to 80 °, with A regular step of 0.05°s^{-1}. Scanning electron microscopy (SEM) images were obtained in a Quanta 200-FEI microscope with 30 kV of applied voltage. The optical absorption spectra were determined with the help of Shimadzu UV-3101 PC equipment within the range 190–900 nm.

Electrical characterization measurements

To perform the electrical measurements on parallel direction to the substrate, the $BiVO_4$ thin film was deposited on non-conductive substrate (soda-lime glass) the same way that was deposited on FTO substrate, as discussed in the previous section. The $BiVO_4$ thin film on soda-lime glass substrate was cut from the same region of the dipped substrate, corresponding to slices of about 1.0 × 2.6 cm perpendicular to the dipping direction. The schematic representations of the sample with the topographic and side view (cross section) are seen in Fig. 1b. The use of an insulating substrate avoids leakage currents through the substrate and allows a configuration measurement perpendicular to the growth direction. As will be seen by SEM images, the rough nature of the deposited film would lead to short circuit channels if the applied voltage was perpendicular to the film surface, in the case that conductive substrates were used. In order to provide a connection to the

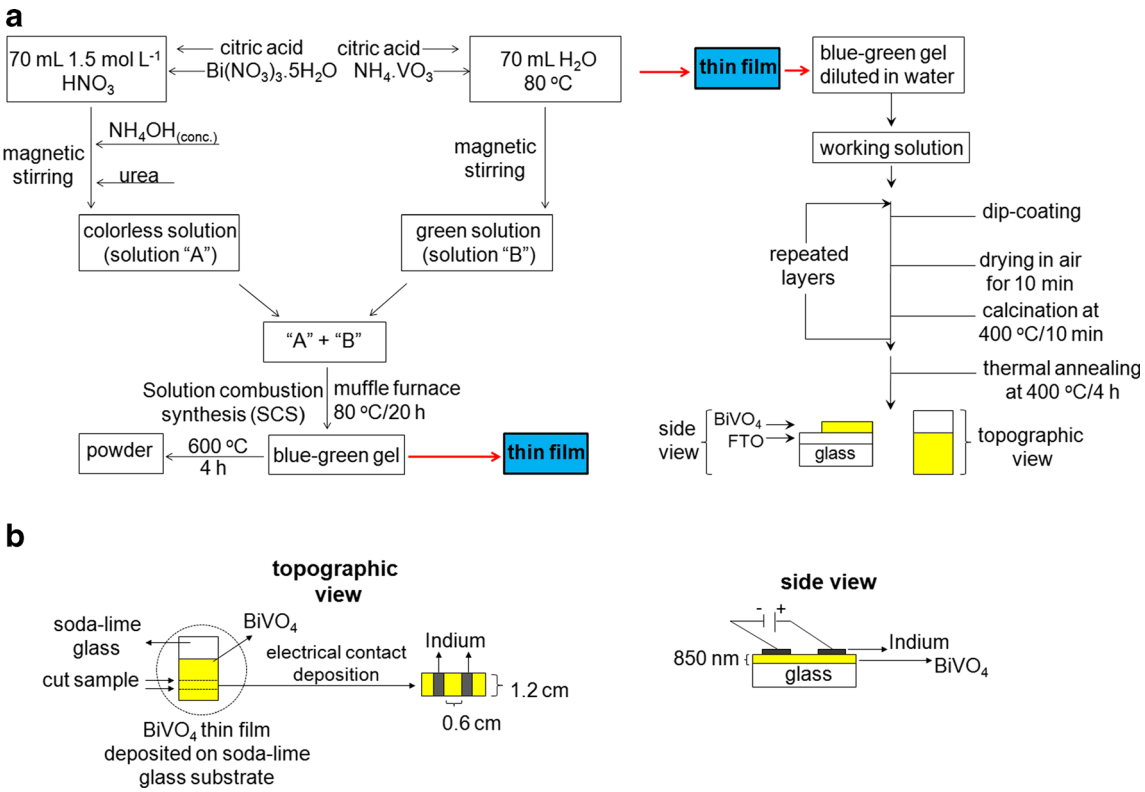

Fig. 1 **a** Simplified diagram showing the solution combustion synthesis (SCS) technique and dip-coating deposition process to obtain monoclinic $BiVO_4$ thin film electrodes. **b** Schematic representations of sample with the topographic and side view (cross section) for the electrical measurements

equipment for the realization of electrical characterization measurements, indium (In) electrical contacts were deposited by the resistive evaporation technique on the $BiVO_4$ films surface. The deposition of indium was carried out in an EDWARDS auto 500 deposition system, under a pressure of about 2×10^{-5} Torr, using tungsten crucibles. The thin film samples were placed very close to each other and the sample holder rotates in order to assure homogeneous deposition of the metallic layer. After metal deposition, the samples were annealed at 150 °C for 30 min. The indium electrodes has been chosen due to the previous best results obtained for oxide semiconductor films [33], concerning its ohmic behavior and low contact resistance. Sample cooling for electrical measurements was performed in a He closed-cycle cryostat from APD cryogenics, coupled with a Lake Shore Cryotronics temperature controller with (0.05 °C precision). The applied bias and the electrical current were measured on a Keithley Electrometer model 6517 A.

Photoelectrochemical measurements

Conventional electrochemical cell with three electrodes were used for the photoelectrochemical experiments, where an Ag/AgCl (3 mol L^{-1} KCl) electrode is the reference, a platinum wire (10 cm in length and 0.5 mm in diameter) is the counter electrode, and the $BiVO_4$ thin film, deposited on FTO conductor substrate, FTO/$BiVO_4$ electrode is the work electrode (the geometrical electrode area in contact with the solution is set to 1 cm^2). Distinct visible light source were used to verify the possibility of charge carrier excitation on $BiVO_4$ thin film: (1) a Philips dichroic lamp with a power of 50 W at an applied voltage of 12 V (this light source presents wide spectra from $\lambda \geq 400$ nm), (2) a blue InGaN light emitting diode (LED) with average wavelength of 450 nm and average power of 15 mW. It must be mentioned that illumination was done on the $BiVO_4$ surface, frontal to the electrode system. The photoelectrochemical characterization procedures are carried out by cyclic voltammetry and chronoamperometry techniques, through a potentiostat/galvanostat Autolab 84,057, version 4.9, using 5 mL of 0.1 mol L^{-1} potassium chloride (KCl) as electrolyte solution.

For the methylene blue (MB) degradation tests, 5 mL was used (10 mmol L^{-1}) in KCl electrolyte solution (0.1 mol L^{-1}). The MB degradation evaluation was carried out by chronoamperometry technique, with controlled potential of +1.4 V during different degradation times. The photoelectrochemical degradation was carried out submitting to visible light irradiation from the dichroic lamp and the InGaN LED, whereas the electrochemical degradation was done in dark conditions. After degradation, the UV–Vis spectra

of the remaining solution were taken and used to verify the relative (percentage) amount of MB that had vanished. The adopted parameter was the decreasing of the MB optical absorption band, taken at approximately 665 nm. These spectra were taken just after the chronoamperometry measurements by Shimadzu UV–3101 PC spectrophotometer.

Results and discussion

Physical and electrical characterization

The x-ray diffractograms results to $BiVO_4$ powder (black line), $BiVO_4$ thin film deposited on soda-lime glass substrate (red line), $BiVO_4$ thin films deposited on FTO substrate (blue line), and only the FTO substrate (green line) are shown in Fig. 2. The monoclinic phase of $BiVO_4$ powder, obtained by calcination of blue-green gel at 400 °C/4 h, is observed as diffracted peaks, shown in Table 1, according to the file (PDF 75–1867) from PCPDFWIN software, version 2.4, JCODS-ICDD. The dip-coating deposition thin film process, adopted in this paper, leads to the monoclinic $BiVO_4$ phase formation as observed by the diffractogram profile. The diffracted peaks seen in Table 1 confirm the monoclinic $BiVO_4$ phase thin film on soda-lime glass substrate. The diffractogram for the film deposited on glass substrate allows identifying only peaks related to $BiVO_4$ phase because the substrate is an amorphous glass, whereas the film deposited on FTO substrate leads to a diffractogram where, besides the $BiVO_4$ peaks, the FTO diffracted peaks can be also identified. The obtained diffraction patterns are in good agreement with previously published reports, with samples either in the form of powders [23, 27–29], as nanocrystalline thin film [7, 10, 16, 18], obtained by solution combustion synthesis (SCS) technique.

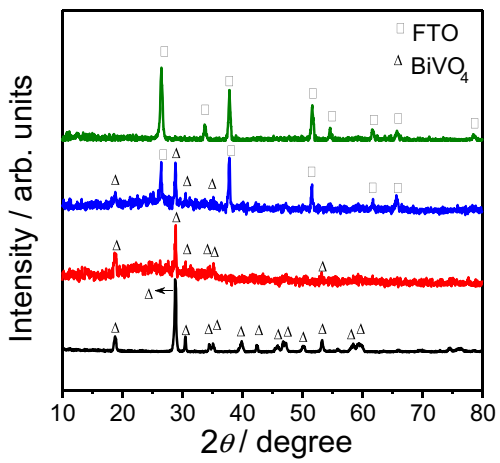

Fig. 2 X-ray diffractogram patterns of $BiVO_4$ thin film deposited on conductive FTO (*blue line*) and non-conductive soda-lime glass substrates (*red line*). Besides, it is also shown the diffraction profile of the $BiVO_4$ in the powder form (*black line*) and FTO substrate (*green line*)

SEM topographic image of $BiVO_4$ film deposited on FTO substrate can be seen in Fig. 3a. The surface image is quite homogeneous, being formed of round-shaped particles homogeneously distributed throughout the investigated area. Concerning the cross-section image (inset in Fig. 3a), the film thickness (about 850 nm) can be assumed as rather uniform. Figure 3b shows the SEM image of a $BiVO_4$ sample in the powder form. Round-shaped particles are clearly observed, homogeneously distributed throughout the investigated area. In this case, there is basically a multimodal distribution of particles, with average size ranging from approximately 100 to 900 nm. Besides, the comparison between the $BiVO_4$ particles from thin films and in the powder form, are quite similar as seen in Fig. 3a, b, except for the particle size which is slightly larger for the powder. This difference is probably related to the final thermal annealing, which is carried out at higher temperature for the powder (600 °C for 4 h), than for the film (400 °C for 4 h).

UV–Vis optical absorption data, recorded for the $BiVO_4$ thin film deposited on FTO substrate, are shown in Fig. 4, along with the bandgap evaluation shown in the inset. The fundamental absorption edge starts at about 540 nm, which is in the visible region of electromagnetic spectrum. Considering direct band gap transition [9], the value of the band gap for this film can be evaluated, in good approximation, by a plot of $(\alpha h\upsilon)^2$ as function of $h\upsilon$ plot, and taking the crossing of the slope of the linear part with the x-axis [16, 34]. The obtained result yields a band gap value of about 2.4 eV, typical of monoclinic $BiVO_4$ phase, which is in good agreement with reported results for $BiVO_4$ in the form of thin films [7, 16, 18, 19, 22] obtained for SCS technique used here. Aiming to verify the influence of FTO substrate in optical absorption of $BiVO_4$ film, UV–Vis absorbance measurements of the substrate alone was carried out. In this case, it is possible to observe that the FTO substrate does not influence the optical absorption of $BiVO_4$, since the conductive substrate absorbs in the ultraviolet region.

Electrical characterization data is plotted in Fig. 5. Typical current–voltage (I versus V) curve for $BiVO_4$ thin film deposited on non-conductive substrate (soda-lime glass) measured at room temperature in the dark condition is shown (Fig. 5), whereas electrical resistivity as function of temperature in the dark, is shown in the inset of Fig. 5. The I versus V data was collected under pressure of about 1×10^{-5} Torr. The current–voltage curve behavior is linear, assuring an ohmic behavior for the system composed of annealed In contacts plus $BiVO_4$ film, which can be visualized as practically a linear metal–semiconductor–metal (MSM) device. However, even though an 80 V bias was applied on the sample, the current value obtained is very low, approximately 72 nA, indicating the high electrical resistivity of the $BiVO_4$ thin film. The inset in Fig. 5 brings resistivity data in the dark, measured under pressure of about 1×10^{-5} Torr. The procedure is as follows: the

Table 1 Comparison between experimental diffraction data and the literature for $BiVO_4$ semiconductor material and related planes with respective Miller's index (hkl)

Experimental 2-theta			Theoretical 2-theta	Miller's index
$BiVO_4$ powder	$BiVO_4$ film/ soda-lime glass	$BiVO_4$ film/FTO	$BiVO_4$ monoclinic structure	(hkl)
18.78	18.76	18.77	18.63	(101)
28.82	28.80	28.91	28.95	(112)
30.54	30.69	30.49	30.55	(004)
34.52	34.54	–	34.39	(200)
35.31	35.29	35.24	35.30	(020)
39.84	–	–	39.56	(114)
42.40	–	–	42.32	(105)
45.74	–	–	45.58	(213)
46.93	47.24	47.20	47.37	(024)
50.08	–	–	50.30	(220)
53.22	53.14	–	53.31	(116)
58.34	–	–	58.39	(312)
59.52	–	–	59.46	(033)

*Monoclinic $BiVO_4$ structure, PDF 75-1867

temperature is lowered down to 30 K, and then, increased data rate of 5 K/min, and data of resistance were collected every 3 K. The data resistance collected was converted in resistivity value as evaluated from sample dimensions: conduction channel thickness (850 nm), contact width (1.2 cm), and distance between contacts (0.6 cm), which can be verified again by inspection of Fig. 1b. As the temperature is lowered down, an increase of resistivity is observed, a typical semiconductor material behavior, and expected for the $BiVO_4$ material. The obtained electrical measurements are in good agreement with previously published works, using nanocrystalline $BiVO_4$ material [30–32]. For example, in the paper of Rettie and coworkers [32], the authors evaluated the electrical properties of $BiVO_4$ crystal obtained by solid state reaction. The value of resistivity obtained to undoped $BiVO_4$ crystal was approximately equal to 5×10^8 Ω cm. This value of resistivity is slightly lower than the value obtained in the present paper, which was approximately 10^9 Ω cm. However, this high

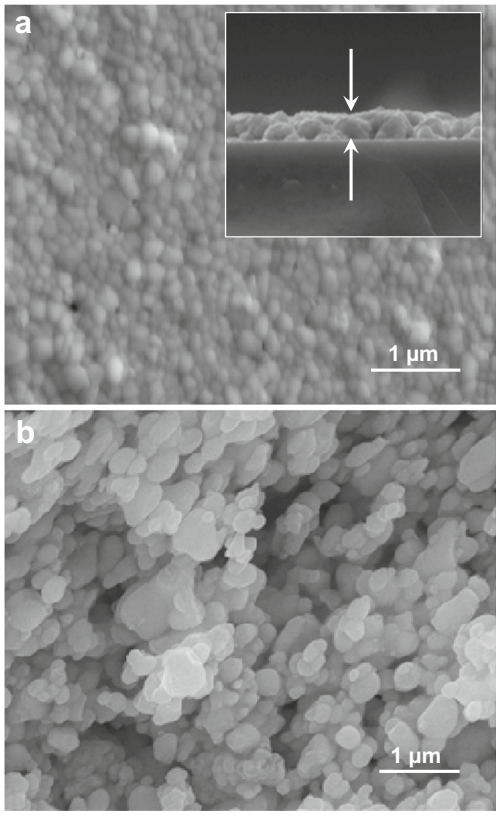

Fig. 3 **a** SEM topographic image of $BiVO_4$ thin film deposited on FTO substrate. *Inset* cross-section image. **b** SEM topographic image of $BiVO_4$ material in the powder form

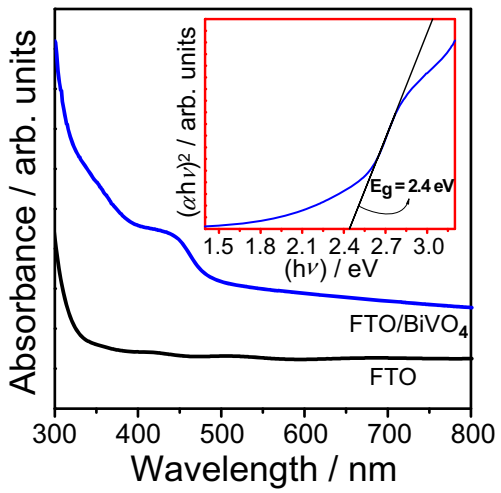

Fig. 4 UV-Vis optical absorption spectra of $BiVO_4$ thin film deposited on FTO. *Inset* direct bandgap evaluation. Besides, it is also shown the UV–Vis optical absorption spectra profile of the FTO substrate

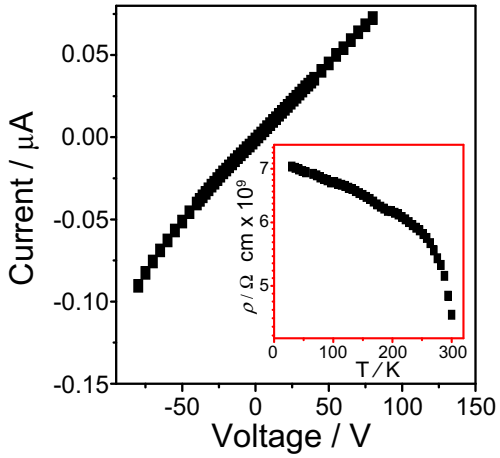

Fig. 5 **a** Current–voltage (*I* versus *V*) curve for $BiVO_4$ thin film deposited on non-conductive substrate (soda-lime glass) measured at room temperature in the dark condition under pressure of about 1×10^{-5} Torr. **b** Resistivity as function of temperature curve, obtained in the dark and under pressure of about 1×10^{-5} Torr conditions

resistivity of $BiVO_4$ thin film is not considered a problem for photoelectrocatalysis measurements. In this case, even with a high electrical resistivity, the increase of charge carrier concentration takes place because electrons and holes are generated by sample photo-excitation process. Besides, the external potential applied in the photoelectrochemical system causes a decrease of electron-hole pair recombination process and, consequently, lead to greater efficiency in the system, as will be shown.

Electrochemical and photoelectrochemical measurements

Figure 6a shows the cyclic voltammograms of $BiVO_4$ thin film in 6.6×10^{-4} mmol cm^{-3} potassium ferricyanide ($K_3[Fe(CN)_6]$) solution. The data were collected at various potential sweep rates (5, 10, 20, 30, 40, 50, 75, and 100 mV s^{-1}). Electrochemical and photoelectrochemical measurements are accomplished for $BiVO_4$ thin film deposited on FTO conductive substrate. From the voltammograms of Fig. 6a and using the Randles–Sevcik equation [35], shown below (Eq. 1), the active area of the electrode was estimated.

$$I_p = \left(2.69 \times 10^5\right)\ n^{3/2}\ A\ D^{1/2}\ C^* v^{1/2} \quad (1)$$

where I_p correspond to the anodic peak current, n is the number of electrons transferred per ion (in this case is equal 1), A is the surface active area of the electrode, D is the diffusion coefficient (equal to 6.7×10^{-6} cm^2 s^{-1}), ν is the scan rate, and C^* is the concentration of $K_3[Fe(CN)_6]$ (6.6×10^{-4} mmol cm^{-3}). The cyclic voltammograms of $BiVO_4$ thin film in potassium ferricyanide solution show that the anodic and cathodic peak currents are proportional to the sweep rate at low values (5–100 mV s^{-1}), which points out to an electrochemical activity of the surface redox transition. The

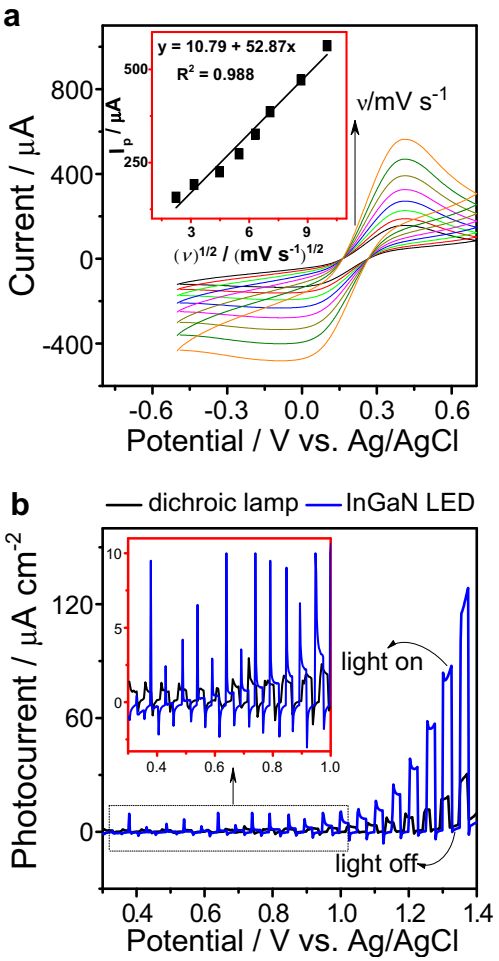

Fig. 6 **a** Cyclic voltammetry profile of monoclinic $BiVO_4$ thin film electrode in 6.6×10^{-4} mmol cm^{-3} $K_4Fe(CN)_6$ at various potential sweep rates from inner to the outer of 5, 10, 20, 30, 40, 50, 75, and 100 mV s^{-1}. *Inset* The linear dependence of anodic leak current with the square root of scan rate. **b** Photovoltammetric profile of monoclinic $BiVO_4$ thin film under chopped visible light from different sources: a dichroic lamp and a blue InGaN LED, both in 0.1 mol L^{-1} KCl solution and $v = 5$ mV s^{-1}

linear dependence of anodic leak current with the square root of the scan rate is inserted in Fig. 6a. The estimated value of the electrode active area is equal to 1.15 cm^2.

Figure 6b shows the photovoltammetric profile of monoclinic $BiVO_4$ thin film under chopped visible light from different sources: a dichroic lamp and a blue InGaN LED. This measurement was carried out by cyclic voltammetry in 0.1 mol L^{-1} KCl solution. In this case, only the anodic sweep is being showed. Through the photovoltammograms, it is possible to observe that $BiVO_4$ is sensible to visible light, where a current jumps under light irradiation and which decays when the illumination is removed. The increasing anodic photocurrent with increasing positive potential indicates the n-type semiconductor behavior [7, 10, 28]. The inset in Fig. 6b shows that the photo-induced current is gradually increased with the increase of potential (anodic sweep) under visible light

irradiation condition. However, under InGaN LED irradiation, the photo-induced current is about five times higher than dichroic lamp irradiation. For instance, the photo-induced current density values, with applied bias of about 1.35 V, are 118 and 23 μA cm^{-2} to InGaN LED and dichroic lamp, respectively. This higher photo-induced current value obtained under the LED irradiation condition can be understood by inspection of Fig. 7, where the emission spectra of the dichroic lamp as well as of the InGaN LED are plotted, in relative intensity (Fig. 7a) as well as in absolute values (Fig. 7b). The $BiVO_4$ band gap energy is also indicated for comparison. As can be clearly seen, the LED band is narrower, and at higher energy, (in the range 2.7 to 2.8 eV), which is a little above the band gap energy of $BiVO_4$ (about 2.4 eV, as inferred from optical absorption data Fig. 4). Figure 7a shows the relative intensity, where the excitation ranges of energy can be compared, and Fig. 7b shows the absolute intensity, measured exactly under the same conditions. The area under each curve is proportional to the photon flux. Then, the measured current density can be seen under a distinct point of view, being normalized by the photon flux (Φ). Considering that the illuminated area is the electrode active area (1.15 cm^2), which is the same, independent on the light source, the photon flux of the LED source is given by $\Phi_{LED} = k_1$. [area under the spectra (whole band)], whereas the photon flux of dichroic lamp is given by $\Phi_{DICHROIC} = k_1$. [area under the spectra, with

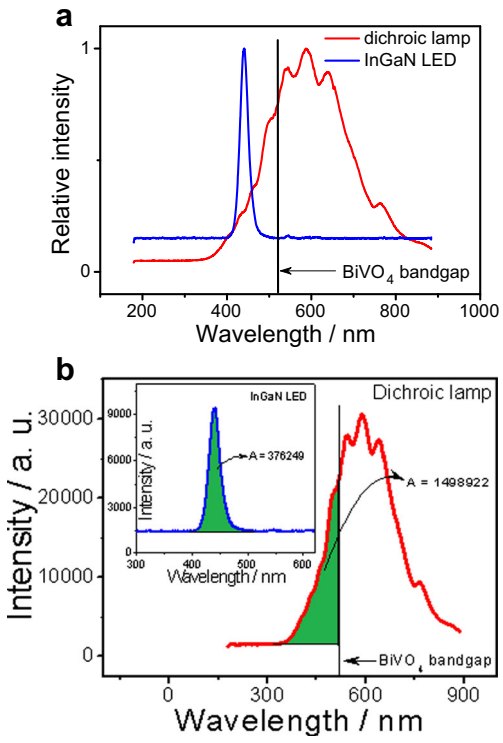

Fig. 7 **a** Relative emission spectra of dichroic lamp and of a blue InGaN LED. $BiVO_4$ band gap is indicated for comparison. **b** Absolute intensity of these source lights. The spectra are measured under the same experimental conditions

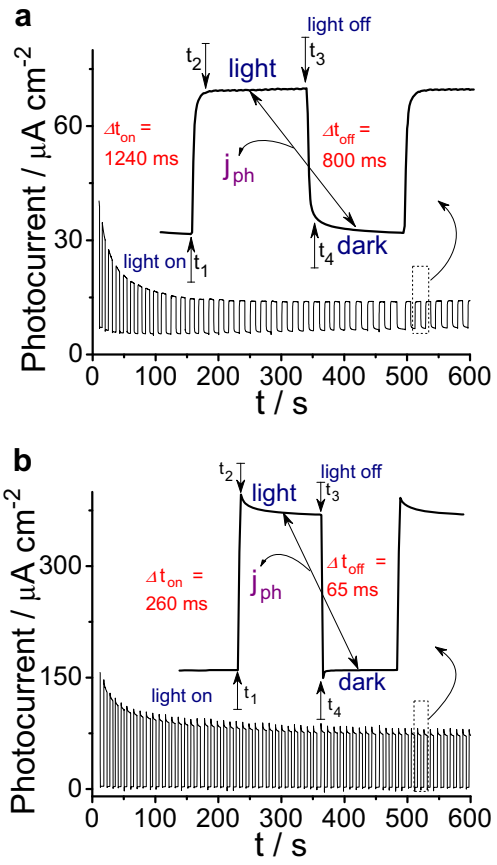

Fig. 8 Photochronoamperogram of monoclinic $BiVO_4$ thin film electrode 0.1 mol L^{-1} KCl solution under chopped distinct visible light irradiation sources. *Inset* details of as were obtained the photoelectrochemical parameters: stability of photocurrent density (j_{ph}), response time (Δt_{on}), and decay time (Δt_{off}) of photocurrent. Controlled potential at +1.4 V versus Ag/AgCl. The visible light sources utilized were **a** dichroic lamp and **b** a blue InGaN LED

energy ≥ bandgap]. In order to compare the current density, the normalized photon flux can be assumed as 1 for the dichroic lamp, since this area is larger, and $\Phi_{NORMALIZED} = \Phi_{LED}/\Phi_{DICHROIC}$, for the LED, which corresponds to the area ratio (0.25). Then, with applied bias of about 1.35 V, the current densities become 472 and 23 μA cm^{-2} to InGaN LED and dichroic lamp illumination, respectively. The excitation of monoclinic phase $BiVO_4$ film with the higher energy of the InGaN LED meets a high density of empty states at conduction band bottom, leading to a greater density of charge carriers. On the other hand, the wide spectra of dichroic lamp (Fig. 7a), with average energy below the $BiVO_4$ band gap, does not

Table 2 Photoelectrochemistry parameters (Δt_{on}, Δt_{off}, and j_{ph}) obtained in KCl electrolyte solution by $BiVO_4$ thin film electrode

Visible light sources	Δt_{on} (s)	Δt_{off} (s)	j_{ph} (μA cm^{-2})
Dichroic lamp	1240	800	7.3
InGaN LED	260	65	284

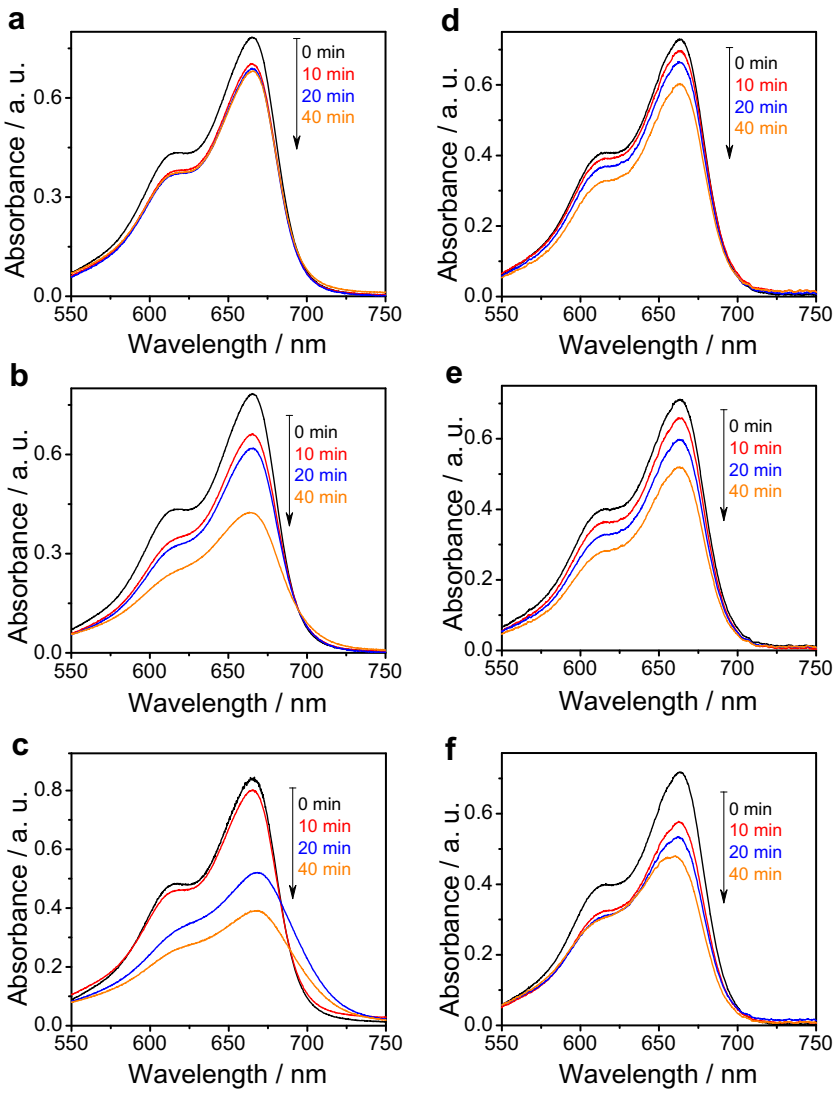

Fig. 9 UV–Vis spectra of MB solution degradation in 0.1 mol L^{-1} KCl using $BiVO_4$ thin film electrode: **a** dark condition, **b** under continuous visible light irradiation condition from dichroic lamp, and **c** under continuous visible light irradiation condition from a blue InGaN LED. UV–Vis spectra of MB solution degradation in 0.1 mol L^{-1} KCl using $BiVO_4$ material in the powder form: **d** dark condition, **e** under continuous visible light irradiation condition from dichroic lamp, and **f** under continuous visible light irradiation condition from a blue InGaN LED

concentrate the necessary energy for efficient excitation of $BiVO_4$, even though there is a spectra tail above the $BiVO_4$ band gap energy and a high photon flux, leading to a lower density of charge carriers and consequently, to a lower photo-induced current. In both cases, the action of the applied electrochemical potential in the system leads to the charge separation, where the electrons are injected on the counter-electrode and holes on surface of $BiVO_4$ material [7, 10], but the higher excitation energy in the case of the InGaN LED leads to much more efficient charge carrier generation. Considering comparable integrated power, where the current density is normalized by the photon flux, the InGaN LED presents to a much more efficient process compared to the dichroic lamp illumination.

The stability of photo-induced current (photocurrent density, j_{ph}) was evaluated by chronoamperometry in 0.1 mol L^{-1} KCl solution with a controlled potential at +1.4 V versus Ag/AgCl (3 mol L^{-1} KCl), under chopped visible light irradiation condition. The photochronoamperogram illustrated in Fig. 8a,

Table 3 Kinetic parameters (k_{obs} and degradation at 40 min) obtained from methylene blue solution degradation by $BiVO_4$ material in thin film and powder forms

Experimental condition	$BiVO_4$ thin film		$BiVO_4$ powder	
	k_{obs} min^{-1}	Degradation at 40 min (%)	k_{obs} min^{-1}	Degradation at 40 min (%)
Dark	30×10^{-4}	13	47×10^{-4}	17
Dichroic lamp	149×10^{-4}	46	79×10^{-4}	26
InGaN LED	200×10^{-4}	54	98×10^{-4}	33

b, shows the photocurrent decay profile of electrode under chopped dichroic lamp and blue InGaN LED irradiation condition, respectively. Under dichroic lamp irradiation, a decrease of 35 % in the photo-induced current density (j_{ph}) value is observed during the first 250 s, and after this time, the photo-induced current density acquires stability, remaining stable up to the maximum of 600 s. The j_{ph} value (normalized by the photon flux, as mentioned earlier), that is obtained by the difference between the current reached under illumination (light on) and without illumination (light off) [10], is equal to 7.3 μA cm^{-2}, as shown in Table 2. The irradiation with the blue InGaN LED, in the first 250 s, allows 51 % decrease in the j_{ph}. However, the j_{ph} does not acquire stability at this time, and only after 460 s it becomes stable, with a value equal to 284 μA cm^{-2}, which is approximately 39 times higher than j_{ph} obtained under dichroic lamp irradiation.

Other two important photoelectrochemical parameters that can be obtained from the photochronoamperogram curve shape (inset in Fig. 8a, b), are: response time (which in this case was arbitrarily called Δt_{on}) and decay time (called Δt_{off}). The response time of electrode was assumed as the necessary time for obtaining the maximum value of the photo-induced current after the system has been illuminated, and the decay time of photo-induced current was assumed as the necessary time for photocurrent decay back for the dark condition after the light is off. These values are very important concerning the photoelectrochemical behavior for the use of the electrode in technological applications [10, 36]. The evaluated value of these parameters is shown in Table 2. It is observed that the response time of electrode is faster when illuminated with the InGaN LED (1240 and 260 ms, for dichroic lamp and InGaN LED, respectively). The decay time of photo-induced current is also faster when the electrode is illuminated with the LED, 800 and 65 ms, for dichroic lamp and InGaN LED, respectively. The photocurrent transient curve shape is a typical fingerprint of electron-hole recombination-back processes at $BiVO_4$ thin film surface [36]. Furthermore, from the obtained photoelectrochemical parameters, it is possible to conclude that the choice of adequate visible light sources is fundamental to obtain the best response from $BiVO_4$ thin film electrode.

The performance of the $BiVO_4$ thin film electrode was also investigated by using a 10 mmol L^{-1} MB solution in 0.1 mol L^{-1} KCl electrolyte solutions. MB degradation analysis was performed by the chronoamperometric technique at +1.4 V versus Ag/AgCl controlled potential. The electrochemical degradation was evaluated in the dark, only by the applied potential, and the photoelectrochemical degradation was carried out under continuous visible light irradiation from the same sources, along with applied potential. The results shown in Fig. 9a–c, correspond to the degradation in dark condition, under continuous visible light from dichroic lamp and under continuous visible light from InGaN LED, respectively. In the dark condition (Fig. 9a), only by the applied external potential effect, the $BiVO_4$ thin film electrode has low degradation percentage of MB solution, only 13 %, as deduced from the decrease of the absorption band intensity of the MB molecule at 665 nm. Under visible light irradiation condition, a high degradation percentage of MB by $BiVO_4$ thin film electrode is observed, in spite of the short electrolysis time (40 min). When the system is irradiated by the dichroic lamp, the degradation percentage is about 46 %, whereas the irradiation with InGaN LED leads to a degradation percentage of 55 %. This superior performance for illumination with InGaN LED can be considered even better when we recall that the photon flux with above band gap energy is higher for illumination with the dichroic lamp. These degradation percentages are summarized in Table 3. The effect of visible light irradiation is quite significant and the degradation percentage under visible light irradiation is considerably larger than the degradation accomplished in the dark. In this case, the

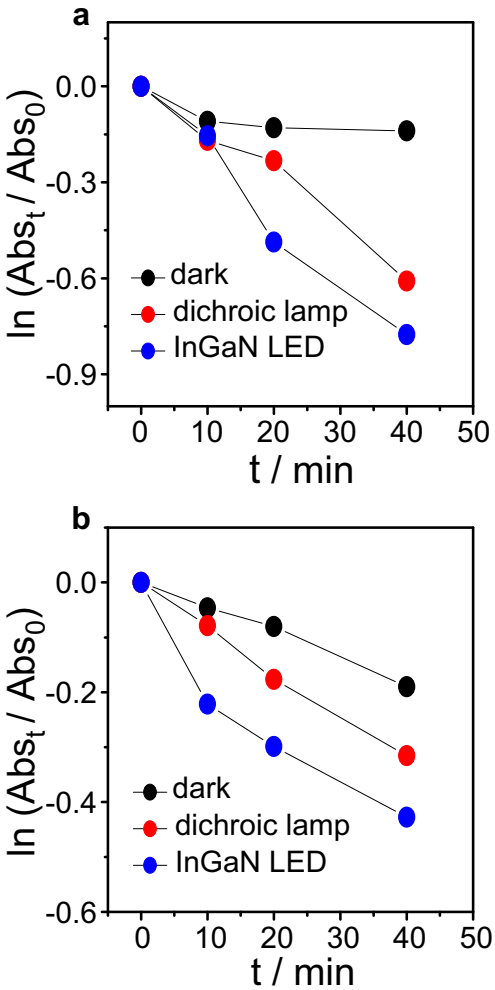

Fig. 10 Decay curves of MB concentration at different degradation times in KCl solution in the dark, under continuous visible light irradiation from dichroic lamp and under continuous visible light irradiation from a blue InGaN LED, conditions: **a** monoclinic $BiVO_4$ thin film electrode and **b** monoclinic $BiVO_4$ powder catalyst

photo-induced effect on the excitation of the semiconductor film, coupled with the external potential applied effect to the working electrode, provides greater system efficiency, due to generation of a higher density of charge carriers and decrease of electron-hole pairs recombination effect. $BiVO_4$ presents n-type conductivity, which means electric conduction done preferentially by electrons. Light irradiation occurs on the film surface and then the photogenerated electrons on the conduction band of $BiVO_4$ may travel through the film width, and are injected on FTO conductor substrate and transferred to the counter-electrode of the electrochemical system. On the other hand, the photogenerated holes on the valence band of the $BiVO_4$ surface have enough lifetime, in order to create a density of holes on the surface relatively high, preventing the fast electron–hole recombination–back process. This high density of surface holes can oxidize water molecules to $^{\bullet}OH$-type radicals that are fundamental in the MB degradation process, due to the attack to the chromophore group of the molecule [7, 10, 27, 37], as already mentioned.

In order to check the catalytic activity of $BiVO_4$ semiconductor material, two tests were realized without applying electrochemical bias: one test under dark condition and another test under visible light irradiation, using dichroic lamp and InGaN LED. $BiVO_4$ powder samples obtained by solution combustion technique were used for these catalytic tests. Tests were performed in a conventional photocatalytic quartz cell under magnetic stirring, inside a wooden box (60 × 60 × 60 cm) coated with an aluminum foil. The visible light sources (dichroic lamp and InGaN LED) were positioned inside the box at a distance of 20 cm from the photocatalytic cell. Then, 10 mmol L^{-1} MB in 0.1 mol L^{-1} KCl electrolyte solution and 1 g L^{-1} of $BiVO_4$ catalyst were used. Figure 9d shows the catalytic activity of $BiVO_4$ powder through the absorption spectra of methylene blue degraded solution, where after 40 min, the $BiVO_4$ catalyst can degrade 17 % of MB solution in the dark condition. Under dichroic lamp and InGaN LED irradiation condition, the $BiVO_4$ powder can degrade 27 and 34 % of MB solution, Fig. 9e, f, respectively. These degradation percentages are summarized in Table 3. These results confirm the catalytic activity of n-type $BiVO_4$ semiconductor material to degrade the MB molecule. Comparing the degradation percentage of MB with $BiVO_4$ thin film and $BiVO_4$ powder under visible light irradiation condition, it is possible to observe that with $BiVO_4$ thin film, the degradation percentage of MB is higher than $BiVO_4$ powder. It is related with the applied electrochemical potential to the system, using thin film, which forces the migration of photogenerated electrons to FTO substrate and holes to $BiVO_4$ surface, suppressing the fast electron-hole recombination process and consequently causing the increase of system efficiency [38].

The degradation profile curves, both in the dark and under visible light irradiation, is evaluated though the graphic of ln (Abs_t/Abs_o) as function of time can be seen in Fig. 10a (for $BiVO_4$ thin film). It suggests that both processes follow pseudo-first-order kinetics [7, 10, 27, 28]. The k_{obs} estimated value, which can be obtained from the slope of the ln (Abs_t/Abs_o) as function of time curve, was equal to 149 × 10^{-4} min^{-1} under dichroic lamp irradiation and 200 × 10^{-4} min^{-1} under InGaN LED irradiation, while the dark conditions the

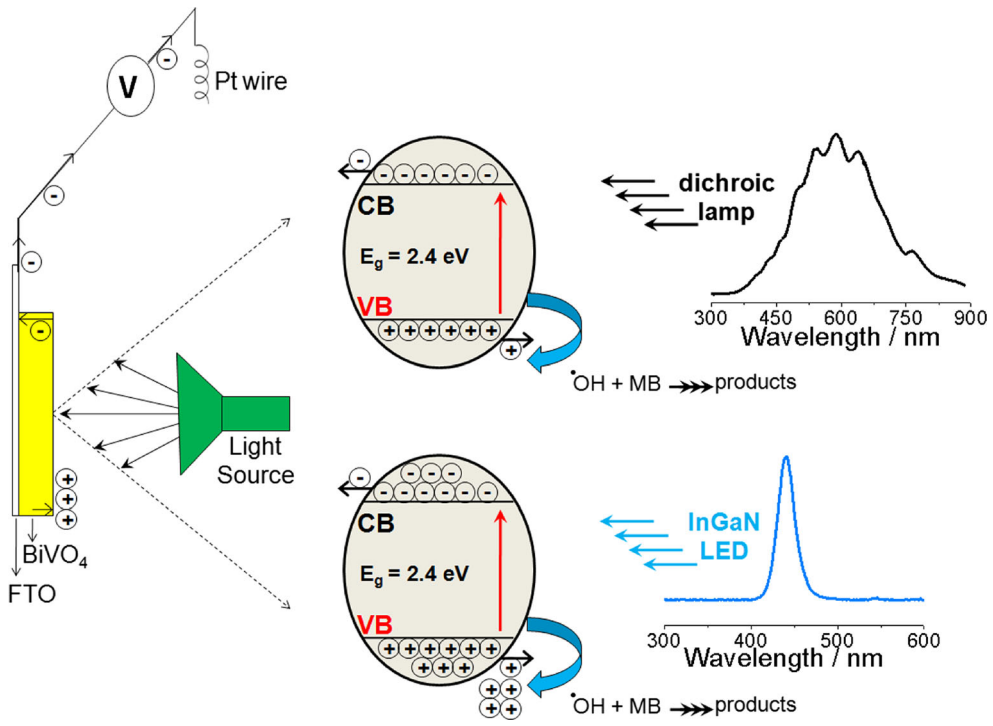

Fig. 11 Schematic drawing illustrating the charge separation diagram of $BiVO_4$ electrode under distinct visible light sources

estimated value of k_{obs} was equal to 30×10^{-4} min^{-1}. The estimated values of k_{obs} are also shown in table 3. It is observed that the rate of MB degradation under visible light effect is higher than the degradation rate in the dark. Considering the $BiVO_4$ powder, which can be seen in Fig. 10b, the k_{obs} estimated value was equal to 79×10^{-4} min^{-1} under dichroic lamp irradiation and 98×10^{-4} min^{-1} under InGaN LED irradiation, whereas in the dark condition, the estimated value of k_{obs} was equal to 47×10^{-4} min^{-1}. In conclusion, it was observed that under InGaN LED irradiation condition, the FTO/$BiVO_4$ electrode showed better performance in MB degradation, as inferred from degradation percentage and estimated k_{obs} values. This better performance can be explained by charge separation diagram illustrated in Fig. 11. In this case, under LED irradiation condition, larger quantities of charge carriers are photogenerated, leading to a larger degradation percentage of MB.

As mentioned before [39, 40], the photocatalytic activity of semiconductor materials can be influenced by many factors, in which surface area of electrode, the hydroxyl radical formation on electrode surface, the light irradiation sources used, and charge separation efficiency are considered as some key factors. Considering the results obtained in this paper, it may be concluded that the combination of these key factors must contribute to the excellent catalytic performance of $BiVO_4$ material in the MB degradation reaction.

Conclusions

The solution combustion synthesis technique, concomitant with the dip-coating deposition process, was quite efficient in obtaining monoclinic $BiVO_4$ semiconductor material in the form of thin film and powder, as demonstrated by the characterization measurements carried out by XRD, SEM, and UV–Vis techniques.

Although the $BiVO_4$ thin film has shown high electrical resistivity, in the photoelectrochemical system, this is not considered a problem due to the high photoactivity presented by the electrode. The photoelectrochemical parameters obtained in KCl electrolyte solution show the FTO/$BiVO_4$ electrode efficiency, under distinct visible light sources irradiation condition. InGaN LED irradiation leads the electrode to a better efficiency, fast response time (260 ms), and fast decay time (65 ms), when compared with the irradiation by dichroic lamp. Besides, the photocurrent density (j_{ph}), normalized by the photon flux, obtained under LED irradiation is approximately 39 times higher than the j_{ph} obtained under dichroic lamp illumination.

The performance analysis based on the MB degradation reaction has shown that the $BiVO_4$ material has higher electroactivity under InGaN LED irradiation condition, with estimated k_{obs} value of 200×10^{-4} min^{-1}, which is a little higher than dichroic lamp condition.

Overall, the results presented here allow concluding that $BiVO_4$ thin film deposited on FTO conductive electrode stands as an important methodological tool with technological potential to be used directly in environmental preservation, specifically in the decontamination of surface water and wastewater.

Acknowledgments The authors wish to thank Prof. Margarida J. Saeki for the SEM images. They also acknowledge CNPq, FAPESP, and FUNDAÇÃO ARAUCÁRIA (15585/2010), NEMAN (Pronex, 17378/2009) for financial support.

References

1. Bian Z-Y, Zhu Y-Q, Zhang J-X, Ding A-Z, Wang H (2014) Chemosphere 117:527–531
2. Ma Y, Jiang H, Zhang X, Xing J, Guan Y (2014) Ceram Int 40: 16485–16493
3. Zeng J, Zhong J, Li J, Xiang Z, Liu X, Chen J (2014) Mater Sci Semicond Process 27:41–46
4. Obregón S, Colón G (2014) Appl Catal B 158–159:242–249
5. Hu L, Dong S, Li Y, Pi Y, Wang J, Wang Y, Sun J (2014) J Taiwan Inst Chem Eng 45:2462–2468
6. Lei B-X, Zeng L-L, Zhang P, Sun Z-F, Sun W, Zhang X-X (2014) Adv Powder Technol 25:946–951
7. Silva MR, Dall'Antonia LH, Scalvi LVA, Santos DI, Ruggiero LO, Urbano A (2012) J Solid State Electrochem 16:2016–2025
8. Thalluri SM, Suarez CM, Hernández S, Bensaid S, Saracco G, Russo N (2014) Chem Eng J 245(2014):124–132
9. Walsh A, Yan Y, Huda MN, Al-Jassim MN, Wei SH (2009) Chem Mater 21:547–551
10. Silva MR, Lucilha AC, Afonso R, Dall'Antonia LH, Scalvi LVA (2014) Ionics 20:105–113
11. Zhang Z, Wang W, Shang M, Yin W (2010) Catal Commun 11: 982–986
12. Naya S, Tanaka M, Kimura K, Tada H (2011) Langmuir 27:10334–10339
13. Obregón S, Colón G (2013) J Mol Catal A Chem 376:40–47
14. Lai H-F, Chen C-C, Chang Y-K, Lu C-S, Wu R-J (2014) Sep Purif Technol 122:78–86
15. Ye H, Park HS, Bard AJ (2011) J Phys Chem C 115:12464–12470
16. Berglund SP, Flaherty DW, Hahn NT, Bard AJ, Mullin CB (2011) Phys Chem C 115:3794–3802
17. Kho YK, Teoh WY, Iwase A, Madler L, Kudo A, Amal A (2011) ACS Appl Mater Interfaces 3:1997–2004
18. Sayama K, Nomura A, Arai T, Sugita T, Abe R, Yanagida M, Oi T, Iwasaki Y, Abe Y, Sugihara H (2006) J Phys Chem B 110:11352–11360
19. Saito R, Miseki Y, Sayama K (2013) J Photochem Photobiol A 258: 51–60
20. Luo W, Wang Z, Wan L, Li Z, Yu T, Zou Z (2010) J Phys D Appl Phys 43:405402
21. Dall'Antonia LH, Tacconi NR, Chanmanee W, Timmaji HK, Myung N, Rajeshwar K (2010) Electrochem Solid-State Lett 13: D29–D32
22. Luo H, Mueller AH, McCleskey TM, Burrel AK, Bauer E, Jia QX (2008) J Phys Chem C 112:6099–6102
23. Timmaji HK, Chanmanee W, Tacconi NR, Rajeshwar K (2011) J Adv Oxid Technol 14:93–105

24. Tokunaga S, Kato H, Kudo A (2001) Chem Mater 13:4624–4628
25. Rajeshwar K, Tacconi NR (2009) Chem Soc Rev 38:1984–1998
26. Jiang H, Endo H, Natori H, Nagai M, Kobayashi K (2008) J Eur Ceram Soc 28:2955–2962
27. Afonso R, Serafim JA, Lucilha AC, Silva MR, Lepre LF, Ando RA, Dall'Antonia LH (2014) J Braz Chem Soc 25:726–733
28. Serafim JA, Afonso R, Lucilha AC, Oliveira LA, Silva PRC, Silva MR, Sartori ER, Dall'Antonia LH (2014) Quim Nov. 37:1158–1164
29. García Pérez UM, Sepúlveda-Guzmán S, Cruz AM, Méndez UO (2011) J Mol Catal A Chem 335:169–175
30. Lu T (1986) Steele BCH. Solid State Lonics 21:339–342
31. Sarkar S, Chattopadhyay KK (2012) Phys E 44:1742–1746
32. Rettie AJE, Lee HC, Marshall LG, Lin J-F, Capan C, Lindemuth J, McCloy JS, Zhou J, Bard AL, Mullins CB (2013) J Am Chem Soc 135:11389–11396
33. Ravaro LP, Scalvi LVA (2011) Mater Res 14:113–117
34. Zhou L, Wang W, Liu S, Zhang L, Xu H, Zhu W (2006) J Mol Catal A Chem 252:120–124
35. Prathap MUA, Satpati B, Srivastava R (2014) Electrochim Acta 130:368–380
36. Long M, Cai W, Kisch H (2008) J Phys Chem C 112:548–554
37. Naya S, Tanaka M, Kimura K, Tada H (2011) Langmuir 27:10334–10339
38. Silva MR, Scalvi LVA, Neto VSL, Dall'Antonia LH (2015) J Mater Sci Mater Electron 26:7705–7714
39. Fan HM, Wang DJ, Wang LL, Li HY, Wang P, Jiang TF, Xie TF (2011) Appl Surf Sci 257:7758–7762
40. Zeng J, Zhong J, Li J, Xiang Z, Liu X, Chen J (2014) Mater Sci Semicond Process 27:41–46